Spectrochimica Acta Part A: Molecular and Biomolecular Spectroscopy 238 (2020) 118392

Contents lists available at ScienceDirect

Spectrochimica Acta Part A: Molecular and Biomolecular Spectroscopy

journal homepage: www.elsevier.com/locate/saa

Simultaneous quantitative analysis of K^+ and Tl^+ in serum and drinking water based on UV–Vis spectra and chemometrics

Lijuan Huang, Longyan Xiang, Yan Zhang, Yongan Wang *, Zhiyong Nie *

State Key Laboratory of Toxicology and Medical Countermeasures, Institute of Pharmacology and Toxicology, Academy of Military Medical Sciences, Beijing 100850, China

ARTICLE INFO

Article history:
Received 28 December 2019
Received in revised form 6 April 2020
Accepted 19 April 2020
Available online 30 April 2020

Keywords:
K^+/Tl^+ detection
Gold nanoparticles
Peroxidase-like activity
Colorimetric reaction
Chemometrics

ABSTRACT

The simultaneous detection of K^+ and Tl^+ can serve as a toxicological diagnostic tool for thallium poisoning. Colorimetric-reaction-based nanoprobes have emerged as promising sensors for the rapid and ultrasensitive detection of molecular species in simple systems. However, the development of viable screening tools for multicomponent analysis in complex systems remains challenging owing to interference from coexisting materials in the media. Herein, a simple chemical sensor array based on the peroxidase-like activity of gold nanoparticles modified with single-stranded DNA (AuNPs-ssDNA) and chemometrics was developed for the simultaneous detection of K^+ and Tl^+ in aqueous solutions and serum. The use of a K^+ adapter conferred high selectivity to the developed method. Optimized AuNPs-ssDNAs were used to construct a sensor array, which together with chemometrics provided fingerprints that can facilitate the simultaneous analysis of multiple components. The developed colorimetric reaction in combination with the chemometrics assay was directly used as a biosensor array, which exhibited detection limits of 107.33 nM for K^+ and 19.26 nM for Tl^+. The developed method could potentially serve as a diagnostic technique for investigating thallium poisoning and toxicology.

1. Introduction

Thallium and its compounds are some of the most toxic heavy metal species and are even more toxic than lead and mercury, which are located adjacent to thallium in the periodic table [1]. Thallium exists in +1 and +3 oxidation states; however, as Tl^+ species are more abundant in the environment, they are the focus of this work. Thallium salts are colorless and tasteless, which make them difficult to detect when drinking and eating. Owing to these characteristics, thallium salts have been widely used as potent poisons in terrorist attacks in several countries, and thallium poisoning by acute intake or chronic exposure has been reported [2,3]. With the ever-increasing growth in mining, an increasing amount of thallium is entering the environment as soluble thallium ions, which can travel deep into the soil, be absorbed by crops, and eventually reach the human body through the food chain [4]. Currently, there are no standard clinical treatments available for deliberate thallium poisoning or environmental thallium pollution exposure. Acute thallium poisoning is rapid, dangerous, and may cause multiple organ dysfunction syndromes and other serious health complications [5]. Unfortunately, both the misdiagnosis and mortality rates of thallium poisoning are very high, and the pathogenesis of thallium poisoning is unclear. The accepted mechanism of action for thallium poisoning is competitive inhibition with K^+. K^+ and Tl^+ have similar ionic radii (Tl^+: 1.54 Å, K^+: 1.44 Å), the same charge, and can be substituted for each other in their mineral salts and in some biological reactions. For example, Tl^+ can replace Na^+ and K^+ in the glutamate transporter excitatory amino acid carrier and in quadruplex DNA [4,6]. Despite these issues, sensing methods for Tl^+ are underexplored compared with those for other elements that belong to the same group in the periodic table, such as lead and mercury. Hence, the simultaneous quantitative analysis of K^+ and Tl^+ in blood is highly important because it could facilitate the rapid and convenient detection and quantitation of Tl^+ poisoning.

The analysis of K^+ and Tl^+ in blood and aqueous solutions has been intensively investigated using sophisticated techniques and instrumentation, such as atomic absorption spectroscopy, inductively coupled plasma (ICP)-atomic emission spectroscopy, and ICP-mass spectrometry [7–9]. Additional monitoring methods for thallium have also been summarized in recent reviews [10,11]. However, these approaches suffer from disadvantages such as the non-portability, space-inefficiency, and high cost of the instrumentation and the complexity of the analytical processes. Although a number of alternative methods for the fast on-site detection of thallium have been reported (Table 1), these methods do not take into account that false positives might be caused by K^+.

* Corresponding authors.
E-mail addresses: huanglijuanlmm@sina.com (L. Huang), yanzha@tju.edu.cn (Y. Zhang), yonganw@sina.com (Y. Wang), niezhiyong2018@sina.com (Z. Nie).

https://doi.org/10.1016/j.saa.2020.118392
1386-1425/

Table 1
Comparison of the proposed optical approach with other reported methods for the detection of Tl^+ and K^+.

	Detection methods	Probe	LODs	Selectivity	Application	References
K^+	Fluorescence	G-quadruplex	7 μM	Li^+, NH_4^+, Pb^{2+}, Hg^{2+}, Mg^{2+}, Zn^{2+}, Ca^{2+} and Cu^{2+}	Urine	[30]
K^+	Fluorescence	G-quadruplex Thioflavin T	0.04 mM	Li^+, Na^+, Ca^{2+}, Mg^{2+}, NH_4^+, Cu^{2+}, Co^{2+}, Pb^{2+}, Zn^{2+} and Fe^{3+}	Lake water and urine	[31]
K^+	Chemiluminescence	G-quadruplex	9 μM	Na^+, NH_4^+, Mg^{2+}, Ca^{2+}, Zn^{2+} and Pb^{2+}	Urine	[32]
K^+	Fluorescence	Triple-helix molecular switch	0.014 mM	Na^+, Li^+, NH_4^+, Mg^{2+}, and Ca^{2+}	None	[33]
K^+	Colorimetric	G-Quadruplex-based DNAzyme	0.5 μM	Na^+	None	[34]
K^+	Colorimetric	G-quadruplex AuNPs	5 nM	Ca^{2+}, Mg^{2+}, Na^+, Li^+, Fe^{2+}, Zn^{2+} and NH_4^+	Urine	[35]
K+	Colorimetric	G-quadruplex	1.9 nM	Pb^{2+}, NH_4^+, Li^+, Ca^{2+}, Mg^{2+}, Zn^{2+}, Fe^{2+}, Ba^{2+} and Al^{3+}	Serum	[36]
K^+	Colorimetric	G-quadruplex	2 nM	Na^+, Ca^{2+}, Mg^{2+}, Ba^{2+}, Zn^{2+} and Fe^{3+}	Urine	[37]
Tl^+	Fluorescent and colorimetric	DNA protected gold nanoparticles	4.6 μM	Na^+, NH_4^+, Li^+, Cs^+, Rb^+, K^+	Lake water sample	[38]
Tl^+	Colorimetric	Rhodamine B hydrazide	0.005 mg/mL	None	Urine	[39]
Tl^+	Colorimetric	Amino acid	5.23 nM	Fe^{2+}, Fe^{3+}, Ba^{2+}, Ni^{2+}, Zn^{2+}, Mn^{2+}, Co^{2+}, Cd^{2+}, Cr^{3+}, and Cu^{2+}	Drinking water	[40]
Tl^{3+}	Colorimetric	4-(5-Bromo-2-pyridylazo)-5-(diethylamino)-phenol (Br-PADAP) as a complex agent	2.6×10^{-6} M	Cl^-, NO_2^-, CH_3COO^-, NO_3^-, BrO_3^-, Cu^{2+}, Pb^{2+}, Ag^+, Fe^{3+}, La^{3+}, Co^{2+}, Ca^{2+}, Mg^{2+}, SO_4^{2-}, ClO_4^-, Al^{3+}, Zn^{2+}, Ni^{2+}, Mn^{2+}, Cd^{2+}, As^{3+}	River water and tap water samples	[6]

Because the mechanism of action for thallium poisoning is likely competitive inhibition with K^+, the presence of potassium may affect the detection of thallium and produce false positive results.

In recent decades, rapid developments in nanotechnology have contributed to the emergence of colorimetric and other biosensing platforms as viable technologies for the on-site detection of various analytes [12–14]. In particular, gold nanoparticles (AuNPs) have been at the forefront in these approaches due to their well-established synthesis routes, propensity for facile modification, high stability, low cost, low toxicity, and remarkable surface plasmon resonance (SPR) properties, which allow the visual read-out of a sensing event. Many SPR-based sensors have been developed for the analysis of heavy metal ions, peptides, proteins, and nucleic acids [15–17]. However, because AuNPs easily undergo surface functionalization, cross-reactions can occur with small molecules in complex biological systems (e.g., blood, saliva, and urine), which result in poor selectivity for AuNP-based sensing.

To establish a method for efficient on-site detection of K^+ and Tl^+ with high selectivity, we sought to employ the peroxidase-like activity of AuNPs modified with single-stranded DNA (AuNPs-ssDNA) to oxidize 3,3′,5,5′-tetramethylbenzidine (TMB; colorless) to TMB_{OX} (color range from light blue to dark blue). In this approach, the color intensity of the TMB chromogenic solution is related to the catalytic activity of the AuNPs-ssDNA. Additionally, we used a K^+ adapter to improve the selectivity of the method. Using AuNPs-ssDNAs optimized via microadjustments to the sequence of the K^+ adapter, a sensor array was constructed to enable the simultaneous quantitative analysis of K^+ and Tl^+. UV–Vis spectra (350–1060 nm) of the TMB chromogenic solution were collected and multivariate calibration models partial least squares (PLS) [18] and backward interval partial least squares (BiPLS) [19] were established. Using multivariate analysis and the developed sensor array, we simultaneously quantified the ions in a binary K^+/Tl^+ system. Data fusion methods were employed to further improve the prediction accuracy of the chemometric models based on our sensor array. The high selectivity and sensitivity of the sensor array designed in this study for the quantitative analysis of Tl^+/K^+ binary mixtures allows the accurate and quantitative analysis of thallium in the presence of potassium, which has not been specifically discussed in many studies (see Table 1). The developed method is expected to be applicable to other related systems comprising biomolecules and biosensor arrays. These novel sensor arrays have potential as low-cost, convenient solutions for the diagnosis and toxicological evaluation of thallium.

2. Experimental section

2.1. Materials and instruments

Hydrogen tetrachloroaurate (III) trihydrate ($HAuCl_4 \cdot 3H_2O$, ≥99.99%), sodium citrate dihydrate ($C_6H_5Na_3O_7 \cdot 2H_2O$, ≥99%), KCl, $CdCl_2 \cdot 2.5H_2O$, $BaCl_2 \cdot 2H_2O$, $MnCl_2 \cdot 4H_2O$, $NiCl_2 \cdot 6H_2O$, $CuCl_2 \cdot 6H_2O$, $FeCl_3 \cdot 6H_2O$, and $CrCl_3 \cdot 6H_2O$ were purchased from Aladdin Industrial Corporation (Shanghai, China). $TlNO_3$ was purchased from Sigma-Aldrich (St. Louis, MO, USA). The ssDNAs 5′-TGG GGG TGT GGG GGT-3′ (T001), 5′-GGT GGT GGT GGT GGT-3′ (T002), 5′-GTT GTT GTT GTT GTT-3′ (T003), 5′-GGT TGG TGT GGT TGG-3′ (T004), 5′-GGT TGG TGT GGT TGG GGT TGG GGT TGG TGT GGT TGG-3′ (T005), and 5′-GGT TGG TGT GGT TGG TGT GTT TGG TGT GGT-3′ (T006), 5′-GGT TGG TGT GGT TGG TGT GTT TGG TGT GGT-3′ (T006), 5′-GGG GGG GGG GGG GGG-3′ (T007), and 5′-TTT TTT TTT TTT TTT-3′ (T008) were purchased from Sangon Biotechnology Co. Ltd. (Shanghai, China). All reagents were of analytical grade and were used without further purification. All solutions were freshly prepared with ultrapure water obtained from a Direct-Q3 system.

UV–Vis spectra were acquired using a UV5Nano UV–Vis spectrometer (Mettler Toledo Corporation). A constant temperature oscillator (ST70-21ST60-4, Hangzhou Miu Instruments Co. Ltd.) was used to mix the solutions and heat them at 37 °C for 30 min.

2.2. Synthesis of AuNPs

All glassware was thoroughly cleaned with freshly prepared aqua regia (HNO_3/HCl = 1:3, v/v) and then rinsed with deionized water. Subsequently, the glassware was dried in an oven at 100 °C for 2–3 h before use.

AuNPs (13 nm) were synthesized by the reduction of a boiling $HAuCl_4$ solution with trisodium citrate. The details of this process have been reported previously [20]. The concentration of the AuNPs in the colloids was estimated using the Beer–Lambert law. The characteristics of the synthesized AuNPs are shown in the supplementary information (Fig. S1).

2.3. Mixed binary solutions of K^+ and Tl^+

To ensure that the components in the binary mixtures were uncorrelated, a grid scheme was used to design the experimental concentration

sets for the binary mixtures. In this approach, a graph was prepared with the Tl^+ concentration on the *x*-axis and the K^+ concentration on the *y*-axis, and the points at the line intersections were obtained. Further details can be found in the supplementary information (Fig. S2 and Table S1).

2.4. Preparation of chromogenic TMB solution

Solution A was prepared by mixing Na_2HPO_4 (0.2 mol·L^{-1}, 25.70 mL), citric acid (0.1 mol·L^{-1}, 24.30 mL), and H_2O (50.00 mL). Solution B was prepared by mixing TMB (2 mg·mL^{-1} in ethanol, 1 mL), solution A (10 mL), and H_2O_2 (140 μL). The TMB chromogenic solution for the experiments was then prepared by mixing solutions A and B (1:1, v/v).

2.5. Sensor arrays

T001, T002, T003, T004, T005, T006, T007, and T008 were selected as AuNP-surface modification agents. After centrifuging the AuNPs (60 mL) to remove the supernatant, the AuNP solution was diluted to 20 mL with deionized water. The AuNPs (3.6 μL) and different volumes of ssDNAs (3.6, 7.2, 10.8, 14.4, 18, 21.6, 25.2, 28.8 or 32.6 μL of T001, T002, T003, T004, T005, T006, T007, or T008, 100 nM) were mixed, diluted to 35 μL with deionized water, and stored at 37 °C for 30 min. Next, the binary mixed solution of Tl^+ and K^+ was added to the AuNPs-ssDNA solution. After holding this mixture at 37 °C for 30 min, the TMB chromogenic solution (200 μL) was added. After 1 h, the UV–Vis spectrum of each solution was collected after diluting to 600 μL with deionized water. The data analysis is described in the following section. Triplicate measurements were conducted for each concentration pair, and each measurement was considered an independent sample.

2.6. Chemometric methods

The entire data set was randomly split into two subsets comprising a modeling set (80%) and an external test set (20%). To build robust models, latent variable (LV) number selection was conducted by bootstrapping Latin partitions [21]. The bootstrapped Latin partitions were used to evaluate the calibration models. The advantage of bootstrapping Latin partitions is that the relative proportions of the class distributions are maintained between the training and prediction sets. The data set is randomly partitioned so that every object was used only once for prediction. An unbiased evaluation of the calibration models is important for the accuracy of the overall model. This approach is efficient and unbiased because all objects were used for the prediction. The performance of the PLS model was evaluated by means of the square of the correlation coefficient (R^2), the root-mean-square error of cross-validation (RMSECV), the root-mean-square error of prediction (RMSEP), the standard deviation of the root-mean-square error of prediction (SD-RMSEP), and the ratio of the standard deviation of the validation set to the standard error of prediction (RPD).

To build a model with more informative variables, data fusion was applied to construct an augmented matrix. A comparison of two data fusion levels (low-level data fusion and mid-level data fusion) was conducted. The schematics of the different levels of data fusion are illustrated in Fig. S5.

The BiPLS toolbox developed by Leardi and Nørgaard [19] was used in this work for BiPLS modeling. All model optimization and construction processes were carried out using MATLAB (The MathWorks Inc., USA).

2.7. Application

To probe the practical applications of the developed sensor array, the AuNPs-ssDNAs were applied to the quantification of K^+/Tl^+ binary mixture in drinking water and artificial serum samples. For accurate determinations of the K^+ concentrations in serum samples, an artificial serum without K^+ was purchased from InnoReagents Co. Ltd. (Huzhou, China). Since serum samples typically do not contain Tl^+, a known amount of the analytes (K^+/Tl^+) was added to the artificial serum or drinking water to prepare test samples.

As the background interference in drinking water is relatively small, we could directly use the PLS regression models (see Fig. 3(a2) for K^+ and Fig. 3(b2) for Tl^+) for predicting the K^+/Tl^+ concentrations in the drinking water samples. The experimental procedure and working conditions were the same as those mentioned above.

3. Results and discussion

3.1. Sensing mechanism

Horseradish peroxidase (HRP)-catalyzed coloration is a widely used clinical diagnostic method due to its straightforward labeling ability and the requirement for fewer sample tests [22]. Further, this method has been widely used in several biochemical detection projects and immune kits. Recently, functional AuNP-based catalysts have attracted significant interest due to their potential applications in several reactions of both industrial and environmental importance [23]. As promising artificial enzyme candidates, catalytically active nanomaterials (nanozymes) show several advantages over natural enzymes, such as controlled synthesis at a low cost, tunable catalytic activities, and high stabilities under stringent conditions. However, the enzyme mimicking potential of AuNPs for catalyzing the oxidation of TMB with H_2O_2 to generate TMB_{OX}, which displays a light blue color, is limited by the relatively low catalytic activity and stability of AuNPs [24]. Several reports have revealed a strong dependence of the enzyme-like properties of AuNPs on their surface properties [23,25]. For these reasons, ssDNA was employed to modify AuNPs and realize improved catalytic activity. The ssDNA-modified AuNPs (AuNPs-ssDNAs) have several exposed nitrogenous ssDNAs on their surfaces, which confer a higher peroxidase catalysis ability for the oxidation of TMB with H_2O_2, which results in the generation of a dark-blue color and thus allows the colorimetric detection of Tl^+ and K^+. In our experiments, we found that the K^+-binding aptamers (PBS) display high selectivity not only for K^+ but also for Tl^+ (Fig. 4). To achieve the simultaneous detection of Tl^+ and K^+, the base sequence (5′-GGT TGG TGT GGT TGG-3′) was slightly adjusted and optimized, and in this study, we selected T001, T002, T003, and T004 to form a sensor array (AuNPs-T001 + AuNPs-T002 + AuNPs-T003 + AuNPs-T004). In the AuNPs-ssDNAs (AuNPs-T001, AuNPs-T002, AuNPs-T003, and AuNPs-T004), the enrichment of the AuNP surfaces with the highly anionic ssDNAs led to the improved oxidation of TMB, which resulted in the dark-blue color being generated more rapidly (Fig. 1(a) and (b)). Notably, in the presence of the K^+ and Tl^+ targets, the resulting ssDNA–K^+ and ssDNA–Tl^+ binding led to the desorption of ssDNA from the AuNP surfaces. Furthermore, with the increase of the K^+ or Tl^+ concentration, the negative charges on the AuNPs-ssDNA surfaces were reduced, which led to a reduction of the AuNP-based peroxidase-like activity and resulted in the solution color changing from dark blue to light blue. This phenomenon can be used to quantify Tl^+ and K^+. The results presented in Fig. 1 indicate that the peroxidase-like activity of AuNPs is dramatically enhanced following the activation of their surfaces with ssDNA (T001, T002, T003, and T004). In the presence of the K^+ and Tl^+ targets, the ssDNAs (T001, T002, T003, T004) leave the surfaces of the AuNPs in a target-concentration-dependent manner, which results in the decrease of the peroxidase catalytic ability of the AuNPs. Thus, K^+ and Tl^+ can be simultaneously quantified using the AuNPs-ssDNA-catalyzed colorimetric TMB oxidation reaction. The degree of the solution color change is dependent on the concentrations of K^+ and Tl^+, and importantly, this change can be monitored by visual inspection or by UV–Vis spectrometric monitoring.

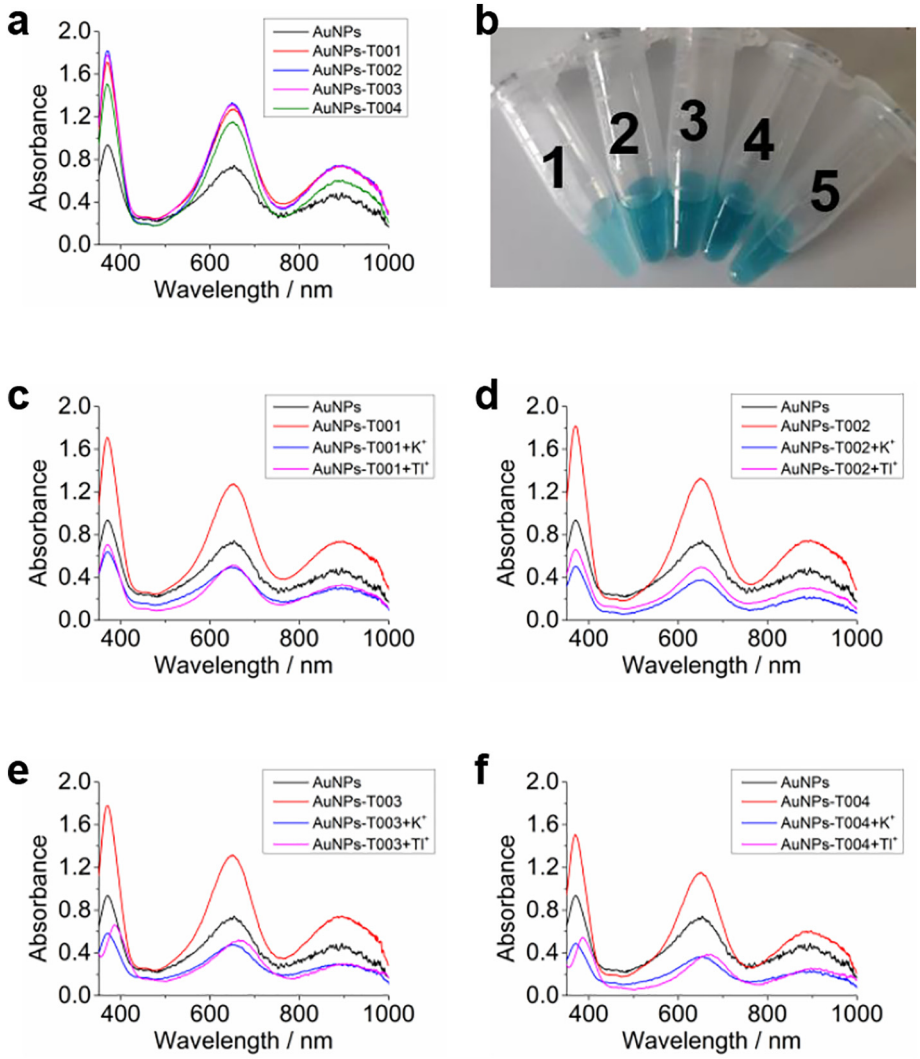

Fig. 1. UV–Vis spectra (a) and photographs (b) of TMB chromogenic solutions in the presence of different nanoenzymes: (1) AuNPs, (2) AuNPs-T001, (3) AuNPs-T002, (4) AuNPs-T003, and (5) AuNPs-T004. Comparison between the UV–Vis spectra of K^+ and Tl^+ with and without different AuNPs sensors: (c) AuNPs-T001, (d) AuNPs-T002, (e) AuNPs-T003, and (f) AuNPs-T004.

The selectivity of the sensor array is determined by the number of sensing elements. To enhance the selectivity and reproducibility of our method, we employed chemometrics (PLS) to analyze the TMB-oxidation-based colorimetry using global UV–Vis spectra (wavelength range: 230–1060 nm) instead of the traditional A_{650} ratio values to increase the number of sensing elements in the sensor array. However, in spectroscopic analyses, some spectral regions may contain information originating from non-modeled interference, background variations, interactions, and other analytes, which often degrade the calibration model and should hence be excluded from the model. Thus, spectral region selection is often required in multicomponent spectroscopic analysis to build a well-fitted model that avoids non-modeled interference. We employed the BiPLS method to further improve the performance of the multicomponent quantitative models.

3.2. Optimization of detection conditions

To select suitable ssDNAs, ssDNAs with different sequences and lengths (T001, T002, T003, T004, T005, T006, T007, and T008) were evaluated. Fig. S3 displays a photograph of the ssDNA-AuNPs sensor array responding to various metal ions (Cu^{2+}, Fe^{2+}, Fe^{3+}, Mn^{2+}, Ni^{2+}, Zn^{2+}, Cd^{2+}, Cr^{3+}, Co^{2+}, Ba^{2+}, Pb^{2+}, K^+, and Tl^+). Among the tested ssDNAs, T001, T002, T003, and T004 displayed better selectivity for K^+ and Tl^+. Therefore, these ssDNAs were used to form a sensor array. The H_2O_2 concentration, temperature, pH, and sensor array detection time are critical determinants of the signal readout (TMB_{OX} color). Furthermore, the catalytic activities of nanozymes (AuNPs and AuNPs-ssDNAs) depend on the operational pH and temperature, and the degree of oxidation relies on the volume of H_2O_2 (30%) used. Therefore, the volume of H_2O_2 (30%) was optimized by incubating the AuNPs and AuNPs-ssDNAs in different volumes of H_2O_2 (90, 100, 110, 120, 130, 140, 150, and 160 μL). Similar to the natural HRP-catalyzed reaction, the AuNPs-ssDNA-catalyzed oxidation of TMB was inhibited at high H_2O_2 concentrations. The results presented in Fig. 2 demonstrate that the maximum A_{650} value is attained when the volume of H_2O_2 (30%) is 140 μL with no further increases observed at higher volumes, which reflects the AuNPs-ssDNA peroxidase catalytic activity. Further, the AuNPs-ssDNAs showed high peroxidase-mimicking activity within the acidic pH range of 4.0–5.0 and between 5 and 30 °C (Fig. 2), which is due to the facile desorption of ssDNA from the AuNP surfaces in strongly acidic or alkaline conditions, or at high temperatures. Notably, this tolerance to acidic pH and low temperature imparts room-temperature operability to our method. The following tests were carried out at 25 °C and pH 4, as the AuNPs exhibit the optimal peroxidase-mimicking activity under these conditions. Fig. 2d

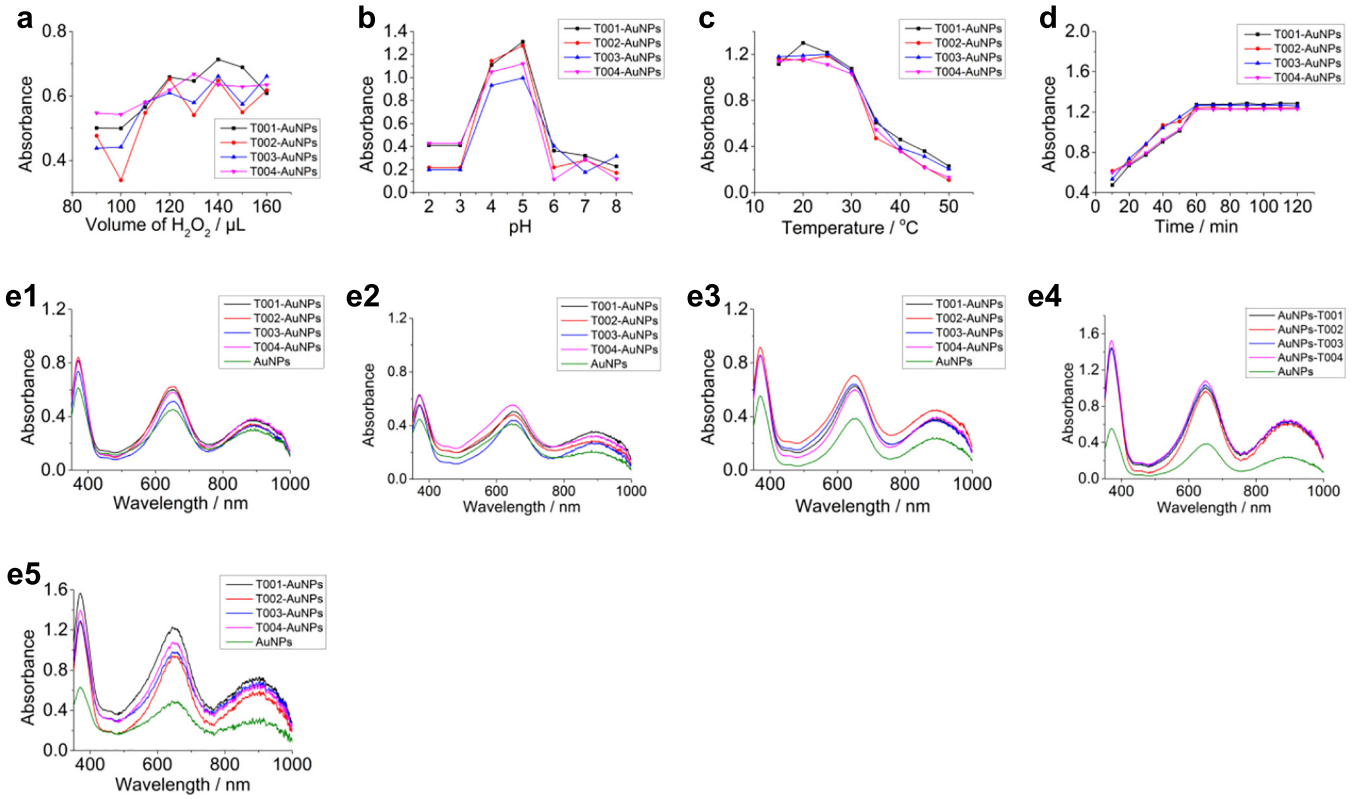

Fig. 2. Absorbance plotted as a function of the volume of H_2O_2 (a), pH (b), temperature (c), and time (d). UV–Vis spectra of TMB chromogenic solutions in the presence of different V_{AuNPs} to V_{DNA} ratios: (e1) 1:1; (e2) 1:2; (e3) 1:3; (e4) 1:4; and (e5) 1:5.

illustrates that the reactions catalyzed by AuNPs-ssDNAs (AuNPs-T001, AuNPs-T002, AuNPs-T003 and AuNPs-T004) achieved equilibrium 1 h.

To achieve higher sensitivity, the spectral difference between the analyses using AuNPs with and without DNA must be as large as possible. To achieve a large spectral difference, we investigated mixing different ratios of the AuNP and ssDNA solutions. Fig. 2e shows the UV–Vis spectra of the chromogenic TMB system in the presence of AuNPs-ssDNA (AuNPs-T001, AuNPs-T002, AuNPs-T003, AuNPs-T004) and AuNPs. The largest differences in the UV–Vis spectra of the chromogenic TMB systems with AuNPs-ssDNA (AuNPs-T001, AuNPs-T002, AuNPs-T003, and AuNPs-T004) and AuNPs were obtained when the ratio between the AuNP and ssDNA solutions was 1:4 (v/v). This optimal condition was used in all subsequent experiments.

3.3. Quantitative analysis of Tl^+ and K^+

The higher peroxidase catalytic activity of AuNPs affords a higher A_{650} value. Further, several methods for the detection of GSH, K^+, H_2O_2, and glucose have been developed based on the A_{650} value [22,26–29]. However, all of the aforementioned methods are specific for the detection of a single analyte and are not suitable for the detection of multiple targets in a mixture. Therefore, the development of a sensitive multisensor colorimetric detection method that allows the simultaneous detection of different ions is of high practical significance. Although establishing a working curve based on the absorbance at characteristic peaks is feasible, the development of a quantitative model based on the full spectrum will afford higher selectivity, tolerance, and reproducibility for practical applications. Thus, we employed a multivariate calibration method (PLS) to quantitatively analyze Tl^+ and K^+ simultaneously. We also employed a data fusion approach to establish quantitative models based on all of the readout signals obtained from different sensing units. Data preprocessing is a necessary procedure before fusing the data sets. Fig. S4 shows the UV–Vis spectra before (a) and after mean centering (b) of the TMB chromogenic solution in the presence of the different nanoenzymes ((1) AuNPs-T001, (2) AuNPs-T002, (3) AuNPs-T003, (4) AuNPs-T004, and (5) AuNPs, as well as (6) data fusion). Fig. S4(b6) shows data set construction. A data set comprising five different data sets based on AuNPs-T001, AuNPs-T002, AuNPs-T003, AuNPs-T004, and AuNPs (75 samples × 3550 wavelengths) was used for building the PLS models.

To eliminate effects from background variations and noise, the spectra were preprocessed using mean, autoscaling, MSC-mean, and MSC-auto. The performance of the PLS model was evaluated using the RMSECV, the square of the correlation coefficient of cross-validation (R^2_{cv}), and the RPD. Within the same concentration range, a higher RPD value indicates higher accuracy. Generally, RPD values > 5 indicate that the model provides acceptable prediction results and values > 8 indicate that the model has a very high prediction accuracy. However, RPD values < 2 indicate that the predicted results are unacceptable. Table 2 summarizes the PLS results (R^2_{cv}, RMSECV, and RPD) obtained

Table 2
PLS models and cross-validation results for the quantitative analysis of the binary K^+/Tl^+ mixture using the sensor array (AuNPs-T001 + AuNPs-T002 + AuNPs-T003 + AuNPs-T004 + AuNPs).

Target	Preprocessed	nLVs	R^2	RMSECV	RPD
K^+	None	10	0.7257	16.95	1.45
	Mean	13	0.9458	8.79	3.08
	Auto	10	0.7184	19.10	1.44
	MSC-mean	13	0.9386	9.55	2.90
	MSC-auto	9	0.8281	15.30	1.78
Tl^+	None	13	0.7976	18.33	1.66
	Mean	13	0.9745	2.66	10.01
	Auto	10	0.9975	6.15	4.38
	MSC-mean	10	0.9736	9.55	2.89
	MSC-auto	10	0.9834	4.96	2.78

from various preprocessed spectra. The obtained R^2_{cv} values indicate that spectral preprocessing is important to improve the performance of the PLS models. The maximum R^2_{cv} value was obtained when the mean was the preprocessed method. Mean centering was employed to increase the differences in the spectra. Importantly, these results allowed us to conclude that even small spectral differences could have a significant impact on our assay. In the subsequent experiments, the mean was used for spectral preprocessing to obtain more robust models. The RPD values obtained for the detection of K^+ and Tl^+ were 3.08 and 10.01, respectively. While the RPD values for Tl^+ and K^+ indicate that this PLS model could quantitatively analyze Tl^+ precisely, its quantitative accuracy for K^+ detection is very poor. This poor performance may be due to the presence of non-modeled information (non-modeled interference, background variations, interactions, and other analytes) in certain spectral regions, which indicates that this information should not be used when preparing the calibration model. Thus, spectral region selection would likely enhance the accuracy of the UV–Vis spectroscopic analysis.

The formation of the sensing array that uses the AuNPs as a sensing unit or the lack of such an array will affect the selectivity and accuracy of the method. Table S2 shows the PLS models and the results of cross-validation based on the sensor array (AuNPs-T001 + AuNPs-T002 + AuNPs-T003 + AuNPs-T004). The R^2_{cv} for detection of K^+ using the sensor array comprising AuNPs-T001 + AuNPs-T002 + AuNPs-T003 + AuNPs-T004 is 0.9330, which is lower than that using the sensor array comprising AuNPs-T001 + AuNPs-T002 + AuNPs-T003 + AuNPs-T004 + AuNPs. This difference in detection is caused by the concentrations of K^+ and Tl^+, which affect the ionic strength of the system and can reduce the stability of the AuNPs. Thus, the catalytic activities of the AuNPs can reflect the concentrations of K^+ and Tl^+. In the subsequent experiments, the AuNPs are also considered as sensor units for the construction of the sensor array.

3.4. Variable selection and data fusion

To improve the quantitative analysis results, BiPLS was used for spectral region selection. BiPLS is a local modeling method proposed by Leardi and Nørgaard [19]. The developed assay may find the optimal spectral regions or their combinations that are suitable and significant for building the calibration model. When BiPLS is used to process spectral data, the processed spectrum is split into several equivalent subintervals (each spectrum was split into 20 UV–Vis spectral subintervals in this study). A series of local PLS models were developed, which were then subjected to backward elimination, wherein the elimination of each interval was evaluated to determine which intervals should be removed to afford the best calibration model. The local PLS model with the lowest RMSECV was selected and regarded as the optimal BiPLS model. When applying both data fusion and variable selection, two strategies are available for building the PLS model. The first is low-level data fusion, in which the data from different sensor units are simply concatenated to set up a data set that is processed by BiPLS. The second is mid-level data fusion, in which a feature data set is extracted from the sensor units by BiPLS to construct a data set that is processed by PLS. Fig. S5 shows the low-level data fusion model (a) and mid-level data fusion model (b).

In low-level data fusion, the UV–Vis spectra of different sensor units are simply concatenated to set up a data set (see Fig. 3(a1) for K^+ and Fig. 3(b1) for Tl^+). First, the UV–Vis spectra of each sensor unit were divided into 20 intervals (the wavelength range of each interval are listed in Table S3) and 100 local calibration models were established. Table S3 summarizes the number of LVs and the RMSECV values of the 100 local calibration models. According to the RMSECV values, model 33 is the optimal model among the 100 local calibration models, 33 intervals (shown in Fig. 3), and 15 LVs employed for K^+ detection. For Tl^+ detection, another 100 local calibration models were established, and the corresponding BiPLS results are also summarized in Table S3. When model 32 was used, the RMSECV value was minimized. Fig. 3(a1) and (b1) illustrate the selected UV–Vis spectral regions (shaded areas) for the detection of K^+ and Tl^+, respectively, and demonstrate the superiority of the results obtained using BiPLS. Fig. 3(a2) for K^+ and Fig. 3(b2) for Tl^+ show the cross-validation and external test results of the BiPLS models. For K^+ detection based on low-level data fusion, the BiPLS model can achieve 3.17 ± 0.18 μM with 10 bootstrap Latin partitions and the R^2_P value reaches 0.9918. For Tl^+ detection based on low-level data fusion, a mean RMSECV of 0.82 ± 0.10 μM is achieved with 10 bootstrap Latin partitions and the R^2_P value reaches 0.9996. The limits of detection (LODs) were calculated based on the IUPAC definition. The LODs of K^+ and Tl^+ in the binary mixture were 20.66 nM and 2.33 nM, respectively. The RPDs of K^+ and Tl^+ in the binary mixture were 11.04 and 50.00, respectively.

For mid-level data fusion, 10 BiPLS models (5 BiPLS models for K^+ and 5 BiPLS models for Tl^+) were built. The optimal spectral intervals (shaded areas) for detection of K^+ (Fig. S6(1)) and Tl^+ (Fig. S6(3)) were selected using each BiPLS model, and the cross-validation results and the external results of the BiPLS models for the detection of K^+ (Fig. S6(2)) and Tl^+ (Fig. S6(4)) based on different nanozymes ((a) AuNPs-T001 (b) AuNPs-T002 (c) AuNPs-T003 (d) AuNPs-T004, and (e) AuNPs) were evaluated. The PLS models and the cross-validation results based on different sensor units (AuNPs-T001, AuNPs-T002, AuNPs-T003, AuNPs-T004, and AuNPs) and the sensor array comprising AuNPs-T001 + AuNPs-T002 + AuNPs-T003 + AuNPs-T004 + AuNPs are listed in Table 3. The results presented in Fig. S6 and Table 3 indicate that an accurate quantitative analysis of K^+ cannot be achieved with any of the sensor units. Therefore, the data fusion technique was applied for further improvement. Next, the feature data set extracted from the sensor units (see Fig. S6(1) K^+ and Fig. S6(3) Tl^+) by BiPLS to construct a data set (see Fig. 3(c1) for K^+ and Fig. 3(d1) for Tl^+) was processed by PLS. To probe the middle level of agreement between the predicted and experimental values, scatter plots of the experimental values and predicted concentrations were obtained from the bootstrapped Latin-partition cross-validation results. The results for the external test sets are shown in Fig. 3(c2) for K^+ and Fig. 3(d2) for Tl^+ along with the precision that is described by the 95% confidence interval obtained by 10 bootstraps. Notably, the predicted K^+ and Tl^+ concentrations are in good agreement with the experimental values based on low-level data fusion. For K^+ detection based on mid-level data fusion, the PLS model can achieve 9.44 ± 0.55 μM with 10 bootstrap Latin partitions and the correlation coefficient reaches 0.9270. For Tl^+ detection based on low-level data fusion, a mean RMSECV value of 1.77 ± 0.12 μM is achieved with 10 bootstraps Latin partitions and the correlation coefficient reaches 0.9978. The LODs of K^+ and Tl^+ in the binary mixture were 107.33 nM and 19.26 nM, respectively. The RPDs of K^+ and Tl^+ in the binary mixture were 3.70 and 21.32, respectively.

These data indicate that better results were obtained by using low-level data fusion since each sensor unit contributes unequally. Therefore, for the current system, low-level data fusion brings together all of the data for comprehensive consideration. Furthermore, the key advantage of low-level data fusion is that the loss of information is minimal.

3.5. Selectivity

Selectivity is a crucial criterion for evaluating the feasibility and merit of a sensor or an analytical method. A selectivity study for AuNPs-T004 has been reported previously [20]. To evaluate the selectivity of the sensor array, we first tested the colorimetric responses toward different metal ions (Cu^{2+}, Fe^{2+}, Fe^{3+}, Mn^{2+}, Ni^{2+}, Zn^{2+}, Cd^{2+}, Cr^{3+}, Co^{2+}, Ba^{2+}, and Pb^{2+}) at a concentration of 100 μM. As indicated by the results in Fig. 4, high selectivities are obtained for the detection of K^+ and Tl^+ using AuNPs-ssDNAs (AuNPs-T001, AuNPs-T002, AuNPs-T003, and AuNPs-T004) in the presence of 13 other metal ions.

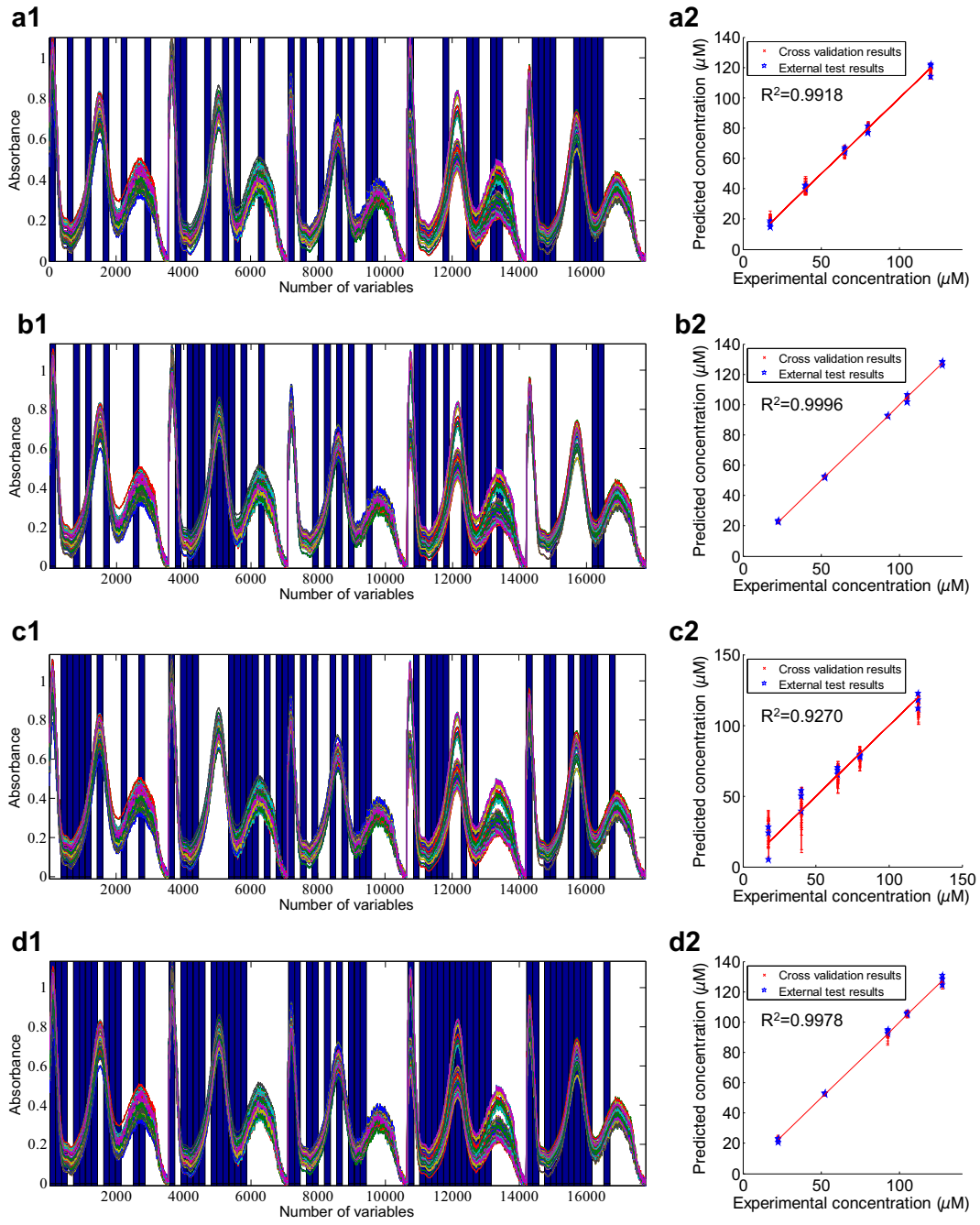

Fig. 3. Optimal spectral intervals (shaded areas) selected by BiPLS for the detection of K^+ (a1, c1) and Tl^+ (b1, d1). Cross-validation and external results of BiPLS models for K^+ (a2, c2) and Tl^+ (b2, d2) based on low-level data fusion (a, b) and mid-level data fusion (c, d).

Table 3
Information about the BiPLS models for the quantitative analysis of the K^+/Tl^+ binary mixture using the sensor units (AuNPs-T001, AuNPs-T002, AuNPs-T003, AuNPs-T004, and AuNPs) and the sensor array (AuNPs-T001 + AuNPs-T002 + AuNPs-T003 + AuNPs-T004 + AuNPs) using mid-level data fusion.

	K^+			Tl^+		
	nLVs	R^2	RMSECV±SD	nLVs	R^2	RMSECV±SD
AuNPs-T001	10	0.5466	23.54 ± 0.74	11	0.9616	7.38 ± 0.98
AuNPs-T002	9	0.3210	28.83 ± 0.58	9	0.9884	4.02 ± 0.12
AuNPs-T003	12	0.7135	18.72 ± 0.92	10	0.9944	2.97 ± 0.17
AuNPs-T004	11	0.6788	19.82 ± 0.75	10	0.9928	3.21 ± 0.13
AuNPs	10	0.6545	20.55 ± 1.00	7	0.9936	3.00 ± 0.12
Sensor array	15	0.9270	9.44 ± 0.55	16	0.9978	1.77 ± 0.12

However, the AuNPs without ssDNA as the nanozyme exhibited poor selectivity for K^+ and Tl^+ detection. Although the presence of several coexisting ions and biomolecules interfere with K^+ and Tl^+ sensing, we investigated the UV–Vis spectral responses of the sensor array, which indicated that corrections could be made for interference between species of interest. The samples studied in the present work contained heavy metals and organic molecules in the serum matrix, and interference from other analytes should be taken into account while other coexisting compounds can be neglected. This aspect of the sensing will be discussed in the following section. Overall, the results from this study show that the combination of the array-based chemical sensor and chemometrics allows simultaneous multicomponent analysis, and any interference between analytes can be corrected using the figure of merit of chemometrics.

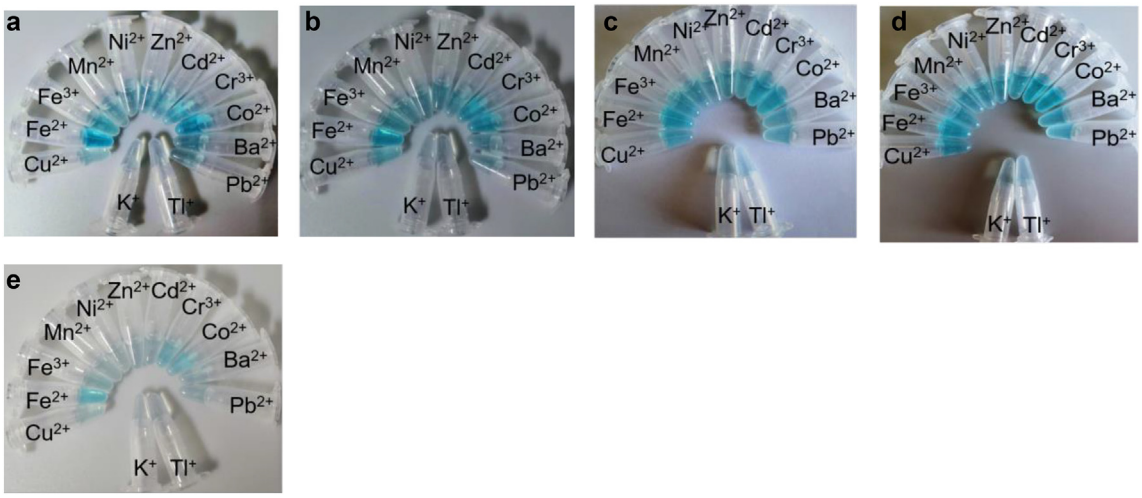

Fig. 4. Photographs of TMB chromogenic solutions containing various metal ions in the presence of different nanozymes: (a) AuNPs-T001, (b) AuNPs-T002, (c) AuNPs-T003, (d) AuNPs-T004, and (e) AuNPs.

Several optical chemical sensors have been developed in previous studies for the analysis of Tl^+ or K^+ (Table 1). Among these methods, our current approach does not have the lowest LODs. However, the previous chemical sensors were applied to the detection of only K^+ or Tl^+. Because the chemical properties of potassium and thallium are similar, it is very difficult to distinguish between them. Therefore, a false positive result may be obtained because the presence of potassium affects the detection of thallium or vice versa. However, the sensor array not only exhibits selectivity for K^+ and Tl^+ in the presence of various metal ions (Cu^{2+}, Fe^{2+}, Fe^{3+}, Mn^{2+}, Ni^{2+}, Zn^{2+}, Cd^{2+}, Cr^{3+}, Co^{2+}, Ba^{2+}, and Pb^{2+}), it can also distinguish thallium from potassium.

3.6. Application

Having optimized the method and studied various approaches for assessing its selectivity, we applied it for the quantification of a K^+/Tl^+ binary mixture in drinking water and artificial serum samples. The PLS model based on low-level data fusion (see Fig. 3(a2) and Fig. 3(b2)) was directly applied for the analysis of the drinking water samples. The recoveries and relative standard deviations (RSDs) of the PLS predictions were 108.21% ± 1.22% for K^+ and 99.86% ± 0.57%, for Tl^+. For serum analyses, as the composition and nature of the external test samples vary greatly, adjustments to the calibration model are required. To address this, we established new calibration models based on low-level data fusion. Fig. 5 shows the UV–Vis spectra of the TMB chromogenic solution for the detection of the binary mixture (K^+/Tl^+) in the group of artificial serum samples based on the sensor array comprising AuNPs-T001 + AuNPs-T002 + AuNPs-T003 + AuNPs-T004 + AuNPs (Fig. 5(a1) and (b1)) and the PLS regression results for K^+ (Fig. 5(a2)) and Tl^+ (Fig. 5(b2)). For K^+ detection based on mid-level data fusion, the PLS model achieved a mean RMSECV value of

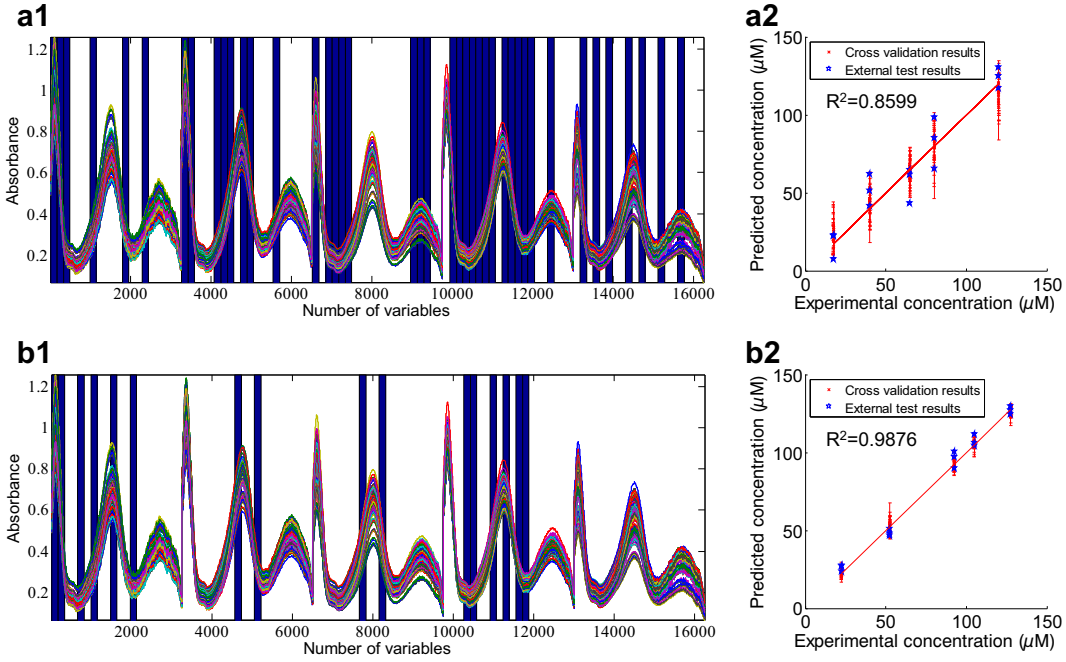

Fig. 5. Optimal spectral intervals (shaded areas) selected by BiPLS for the detection of K^+ (a1) and Tl^+ (b1) in serum based on low-level data fusion. Cross-validation and external results of BiPLS models for the detection of K^+ (a2) and Tl^+ (b2) in serum based on low-level data fusion.

13.08 ± 0.65 μM with 10 bootstrap Latin partitions and the R_P^2 value reached 0.8599. For Tl^+ detection based on low-level data fusion, a mean RMSECV value of 4.17 ± 0.21 μM was achieved with 10 bootstrap Latin partitions and the R_P^2 value reached 0.9876. The LODs for K^+ and Tl^+ in the artificial serum samples were 1.35 μM and 326.44 nM, respectively. The RPDs of K^+ and Tl^+ in the artificial serum samples were 2.67 and 8.98, respectively. Although high background interference was observed for the serum samples, the Tl^+ concentrations predicted by the BiPLS model (RPD > 8) were correct. Simultaneously, the developed method also satisfactorily met the requirements for the semiquantitative analysis of K^+ in serum (RPD > 2). Having made an important advance in this direction, our subsequent research in this area will focus on improving the accuracy and selectivity of this method for the detection of K^+.

4. Conclusion

A straightforward visible-readout chemical sensor array based on the peroxidase-like activity of AuNPs-ssDNAs and chemometrics was developed for the simultaneous detection of K^+ and Tl^+ in serum and water. The ssDNAs were optimized to achieve high selectivity, and the accuracy was improved using chemometric methods (PLS, BiPLS, and data fusion). The LODs of the developed assay were 20.66 nM and 2.33 nM for K^+ and Tl^+, respectively in water, and 1.35 μM and 326.44 nM for K^+ and Tl^+, respectively in serum. Importantly, as the developed assay successfully detected low concentrations of K^+ and Tl^+ in drinking water, it can thereby be used to ensure water safety. The method also allowed the accurate analysis of K^+ and Tl^+ concentrations in serum, which will enable the diagnosis and treatment of thallium poisoning.

CRediT authorship contribution statement

Lijuan Huang: Investigation, Methodology, Software, Formal analysis, Data curation, Writing - original draft, Visualization.**Longyan Xiang:**Resources, Formal analysis, Data curation.**Yan Zhang:**Resources, Formal analysis.**Yongan Wang:**Writing - review & editing, Project administration, Supervision.**Zhiyong Nie:**Writing - review & editing, Project administration, Supervision.

Declaration of competing interest

No conflict of interest exits in the submission of this manuscript, and manuscript is approved by all authors for publication. I would like to declare on behalf of my co-authors that the work described was original research that has not been published previously, and not under consideration for publication elsewhere, in whole or in part. All the authors listed have approved the manuscript that is enclosed.

Appendix A. Supplementary data

Supplementary data to this article can be found online at https://doi.org/10.1016/j.saa.2020.118392.

References

[1] S.F. Xue, Z.H. Chen, X.Y. Han, Z.Y. Lin, Q.X. Wang, M. Zhang, G. Shi, DNA encountering terbium(III): a smart "chemical nose/tongue" for large-scale time-gated luminescent and lifetime-based sensing, Anal. Chem. 90 (2018) 3443–3451.
[2] R. Riyaz, S.L. Pandalai, M. Schwartz, Z.N. Kazzi, A fatal case of thallium toxicity: challenges in management, J. Med. Toxicol. (2012) 1–4.
[3] H. Xu, Y. Luo, P. Wang, J. Zhu, Z. Yang, Z. Liu, Removal of thallium in water/wastewater: a review, Water Res. 165 (2019), 114981. .
[4] R.S. Hoffman, Thallium toxicity and the role of Prussian blue in therapy, Toxicol. Rev. 22 (2003) 29–40.
[5] A.L.J. Petera, T. Viraraghavanb, Thallium: a review of public health and environmental concerns, Environ. Int. 31 (2005) 493–501.
[6] M. Fouladgar, A.A. Ensafi, A novel optical chemical sensor for thallium(III) determination using 4-(5-bromo-2-pyridylazo)-5-(diethylamino)-phenol, Sensors Actuators B Chem. 143 (2010) 590–594.
[7] B. Krasnodębska-Ostręga, J. Pałdyna, M. Wawrzyńska, E. Stryjewska, Indirect anodic stripping voltammetric determination of Tl(I) and Tl(III) in the Baltic seawater samples enriched in thallium species, Electroanalysis 23 (2010) 605–610 (n/a-n/a).
[8] P. Boning, B. Schnetger, Rapid and accurate determination of thallium in seawater using SF-ICP-MS, Talanta 85 (2011) 1695–1697.
[9] N.D. Solovyev, N.B. Ivanenko, A.A. Ivanenko, Whole blood thallium determination by GFAAS with high-frequency modulation polarization Zeeman effect background correction, Biol. Trace Elem. Res. 143 (2011) 591–599.
[10] T. Xiao, F. Yang, S. Li, B. Zheng, Z. Ning, Thallium pollution in China: a geo-environmental perspective, Sci. Total Environ. 421–422 (2012) 51–58.
[11] N. Belzile, Y.-W. Chen, Thallium in the environment: a critical review focused on natural waters, soils, sediments and airborne particles, Appl. Geochem. 84 (2017) 218–243.
[12] L. Zhang, D. Peng, R.-P. Liang, J.-D. Qiu, Graphene-based optical nanosensors for detection of heavy metal ions, TrAC Trends Anal. Chem. 102 (2018) 280–289.
[13] L. Yu, L. Zhang, G. Ren, S. Li, B. Zhu, F. Chai, F. Qu, C. Wang, Z. Su, Multicolorful fluorescent-nanoprobe composed of Au nanocluster and carbon dots for colorimetric and fluorescent sensing Hg^{2+} and Cr^{6+}, Sensors Actuators B Chem. 262 (2018) 678–686.
[14] Z. Wang, L. Ma, Gold nanoparticle probes, Coord. Chem. Rev. 253 (2009) 1607–1618.
[15] F. Chai, C. Wang, T. Wang, L. Li, Z. Su, Colorimetric detection of Pb^{2+} using glutathione functionalized gold nanoparticles, ACS Appl. Mater. Interfaces 2 (2010) 1466–1470.
[16] E. Priyadarshini, N. Pradhan, Gold nanoparticles as efficient sensors in colorimetric detection of toxic metal ions: a review, Sensors Actuators B Chem. 238 (2017) 888–902.
[17] J. Zong, S.L. Cobb, N.R. Cameron, Peptide-functionalized gold nanoparticles: versatile biomaterials for diagnostic and therapeutic applications, Biomater. Sci. 5 (2017) 872–886.
[18] S. Wold, M. Sjostrom, L. Eriksson, PLS-regression a basic tool of chemometrics, Chemom. Intell. Lab. Syst. 58 (2001) 109–130.
[19] R. Leardi, L. Norgaard, Sequential application of backward interval partial least squares and genetic algorithms for the selection of relevant spectral regions, J. Chemom. 18 (2004) 486–497.
[20] By John Turkevich, P.C. Stevenon, J. Hiller, A study of the nucleation and groeth processes in the synthesis of colloidal gold, Discuss. Faraday Soc. 11 (1951) 55–75.
[21] P. Harrington, Statistical validation of classification and calibration models using bootstrapped Latin partitions, TrAC Trends Anal. Chem. 25 (2006) 1112–1124.
[22] Z. Chen, L. Tan, S. Wang, Y. Zhang, Y. Li, Sensitive colorimetric detection of K(I) using catalytically active gold nanoparticles triggered signal amplification, Biosens. Bioelectron. 79 (2016) 749–757.
[23] Y. Lin, J. Ren, X. Qu, Catalytically active nanomaterials: a promising candidate for artificial enzymes, Acc. Chem. Res. 47 (2014) 1097–1105.
[24] B. Hvolbæk, T.V.W. Janssens, B.S. Clausen, H. Falsig, C.H. Christensen, J.K. Nørskov, Catalytic activity of Au nanoparticles, Nano Today 2 (2007) 14–18.
[25] S. Zhang, D. Zhang, X. Zhang, D. Shang, Z. Xue, D. Shan, X. Lu, Ultratrace naked-eye colorimetric detection of Hg^{2+} in wastewater and serum utilizing mercury-stimulated peroxidase mimetic activity of reduced Graphene oxide-PEI-Pd nanohybrids, Anal. Chem. 89 (2017) 3538–3544.
[26] H.H. Deng, G.L. Hong, F.L. Lin, A.L. Liu, X.H. Xia, W. Chen, Colorimetric detection of urea, urease, and urease inhibitor based on the peroxidase-like activity of gold nanoparticles, Anal. Chim. Acta 915 (2016) 74–80.
[27] S. Wang, W. Chen, A.L. Liu, L. Hong, H.H. Deng, X.H. Lin, Comparison of the peroxidase-like activity of unmodified, amino-modified, and citrate-capped gold nanoparticles, Chemphyschem 13 (2012) 1199–1204.
[28] X. Zheng, Q. Liu, C. Jing, Y. Li, D. Li, W. Luo, Y. Wen, Y. He, Q. Huang, Y.T. Long, C. Fan, Catalytic gold nanoparticles for nanoplasmonic detection of DNA hybridization, Angew. Chem. Int. Ed. Engl. 50 (2011) 11994–11998.
[29] Y.M. Wang, J.W. Liu, J.H. Jiang, W. Zhong, Cobalt oxyhydroxide nanoflakes with intrinsic peroxidase catalytic activity and their application to serum glucose detection, Anal. Bioanal. Chem. 409 (2017) 4225–4232.
[30] L. Xu, N. Sun, L. Zhou, X. Chen, J. Wang, Q. Wang, K. Wang, J. Zhang, R. Pei, A label-free fluorescence assay for potassium ions using riboflavin as a G-quadruplex ligand, Analyst 140 (2015) 3352–3355.
[31] X. Sun, Q. Li, J. Xiang, L. Wang, X. Zhang, L. Lan, S. Xu, F. Yang, Y. Tang, Novel fluorescent cationic benzothiazole dye that responds to G-quadruplex aptamer as a novel K^+ sensor, Analyst 142 (2017) 3352–3355.
[32] J. Dong, H. Zhao, F. Zhou, B. Li, Rapid and sensitive detection of potassium ion based on K^+-induced G-quadruplex and guanine chemiluminescence, Anal. Bioanal. Chem. 408 (2016) 1863–1869.
[33] A. Verdian-Doghaei, M.R. Housaindokht, K. Abnous, A fluorescent aptasensor for potassium ion detection-based triple-helix molecular switch, Anal. Biochem. 466 (2014) 72–75.
[34] T. Li, E. Wang, S. Dong, G-Quadruplex-based DNAzyme as a sensing platform for ultrasensitive colorimetric potassium detection, Chem. Commun. (2009) 580–582.
[35] Z. Chen, Y. Huang, X. Li, T. Zhou, H. Ma, H. Qiang, Y. Liu, Colorimetric detection of potassium ions using aptamer-functionalized gold nanoparticles, Anal. Chim. Acta 787 (2013) 189–192.

[36] H. Sun, X. Li, Y. Li, L. Fan, H.B. Kraatz, A novel colorimetric potassium sensor based on the substitution of lead from G-quadruplex, Analyst 138 (2013) 856–862.
[37] Y. Zhang, B. Li, Reducing background signal of G-quadruplex-hemin DNAzyme sensing platform by single-walled carbon nanotubes, Biosens. Bioelectron. 27 (2011) 137–140.
[38] M. Hoang, P.-J.J. Huang, J. Liu, G-quadruplex DNA for fluorescent and colorimetric detection of thallium(I), ACS Sensors 1 (2015) 137–143.
[39] A.S. Parakudyil, A.K. Pillai, S.B. Mathew, Sensitive spectrophotometric determination of thallium(I) using rhodamine B hydrazide in micellar medium, Anal. Methods 3 (2011) 1546.
[40] L. Huang, L. Wang, Z. Nie, Y. Wang, Simultaneous quantitative measurements of Tl^{+} and Pb^{2+} in drinking water based on nanoplasmonic probe, Food Chem. 319 (2020), 126543. .